Probing the metrology- and chemistry-dependences of the onset condition of strong "nanoconfinement" effects on dynamics

Daniel Diaz Vela[1], Asieh Ghanekarade[1], and David S. Simmons[1*]

[1]Department of Chemical and Biomedical Engineering, The University of South Florida, Tampa, FL 33620, USA.

*4202 E. Fowler Ave., ENB 118, Tampa FL 33620, dssimmons@usf.edu

***Abstract*: Polymers in the nanoscale vicinity of interfaces exhibit a broad range of alterations in their dynamics and glass-formation behavior. A major goal in the study of these effects is to understand their strong apparent dependence on chemistry, measurement timescale, and metrology. Here we employ molecular dynamics simulations of thin freestanding polymer films over a range of thicknesses and polymer backbone stiffnesses to probe these dependences. Results suggest that a chemistry and metrology dependent onset of strong nanoconfinement may play an important role in chemical and metrological variations in the apparent strength of nanoconfinement effects. Beyond this onset, we find that the activation barrier for relaxation is subject to a simple temperature-insensitive rescaling near a surface at low temperatures, leading to a fractional power law decoupling relationship between thin film and bulk dynamics. We show that a generic two-barrier model of the glass transition can parsimoniously describe much of this phenomenology, with the 'onset' of strong interface effects on dynamics related to a crossover in dominance from a high temperature barrier to a low temperature barrier. We suggest that variation of this onset timescale and temperature may play an important role in system-to-system and measurement-to-measurement variations in the observed strength of interfacial effects on dynamics and glass formation. These results may also explain why simulations at relatively short timescales commonly report effects of a magnitude comparable to experiments at much larger timescales.**

Introduction

One of the central open questions in the study of nanostructured materials over the last 25 years has been the nature and origin of observed alterations in the dynamics and glass formation of soft materials in the nanoscale vicinity of interfaces[1–10]. From both a fundamental and practical standpoint, a major challenge in this field is a lack of understanding of how the magnitude of these effects depends upon chemistry and relaxation function. Practically, these issues are relevant to the design of materials with targeted interfacial dynamics and mechanics. Fundamentally, the question of why distinct chemistries have differential susceptibilities to interfacial alterations in dynamics may be relevant to the understanding of the underlying physics of glass formation.

Near-interface alterations in dynamics and glass formation can be strikingly large in magnitude, with shifts in the glass transition temperature T_g of order 50 K observed in films of readily accessible thicknesses (> 10 nm) and shifts as high as 100 K or more observed in the extreme limit of films well under 10 nm in thickness[11–13]. The dependence of the magnitude and direction on the nature of the confining interface has become better phenemenologically understood over the last 5 years: the relative high-frequency modulus of the confining interface and the strength of attractive interactions between confined material and substrate play central roles in determining these outcomes[4,14,15].

However, there is a much poorer understanding of the dependence of the strength of these 'nanoconfinement' effects on the chemistry and structure of the confined material itself. The susceptibility of liquids to interfacial perturbations in T_g appears to vary considerably with chemistry, with this susceptibility sometimes[16–18], but not always[19–21], correlated with fragility of glass formation. For example, in simulation and experiment, increased chain stiffness appears to correlate with suppression of nanoconfinement effects, although it is also associated with an increase in bulk fragility[19,21]. As another example, in simulation, introduction of dihedral potentials to polymer models can suppress interfacial alterations in simulated dielectric relaxation over the time scale accessible to these simulations[22].

In addition to chemistry, the magnitude and direction of observed alterations in dynamics and glass formation near interfaces can also depend on the manner by which these alterations are measured. Examples include differences in dynamical trends inferred from ellipsometry, fluorescence, dielectric spectroscopy, and neutron scattering [23–33]. Some of these differences may be explained by variations in the manner by which distinct metrologies average or weight over underlying gradients in dynamics[23–25,31–40]. However, this explanation of metrological dependences in terms of weighting effects has been shown most directly to apply when comparing dynamic to pseudo-thermodynamic measurements[34]. It is not clear that gradient average weighting effects can account for other apparent metrological dependences, such as apparent differences in the

strength of interfacial alterations in distinct dynamical relaxation functions. For example, work by Shavit and Riggleman has demonstrated the presence of differential alterations in near-interface dynamics when they are quantified via translational vs reorientational relaxation functions[19]. This combined dependence of nanoconfinement effects on chemistry and metrology has challenged the determination of underlying relationships between chemistry and susceptibility to interfacial perturbations of dynamics and glass formation behavior.

One potential organizing principle for this variation is suggested by a decade of work pointing to the presence of an *onset* condition of strong interfacial perturbations in dynamics. This onset condition has been inferred in experiment from ellipsometry experiments of Fakhraai and coworkers performed over a range of cooling rates[41–44]. Thin film relaxation rates inferred from these measurements are found to obey a roughly Arrhenius temperature dependence to within the uncertainty in the data (see Figure 1a); an upward extrapolation of these Arrhenius fits suggests an approximate "onset" condition at which thin film dynamics extrapolate back to bulk on heating. For these ellipsometry data, the onset is generally reported to be thickness-independent to within experimental uncertainty for the film thicknesses they have probed, although examination of the surface embedding and nanohole relaxation in Figure 1a suggests that the onset is higher (or is poorly captured by the Arrhenius extrapolation from much lower-temperature data) for relaxation immediately at the surface (see the circled leftmost points for surface embedding and nanohole relaxation in Figure 1a).

An onset is also present in film viscous response data of Tsui and coworkers[45], although their data do not appear to have been discussed in this language until recently[1]. As shown in Figure 1b (reproduced from Tsui and coworkers[45]), for any given film thickness $h > 5$ nm, there exists a temperature above which (relaxation timescale below which) a recovery of bulk-like viscous response is directly observed.

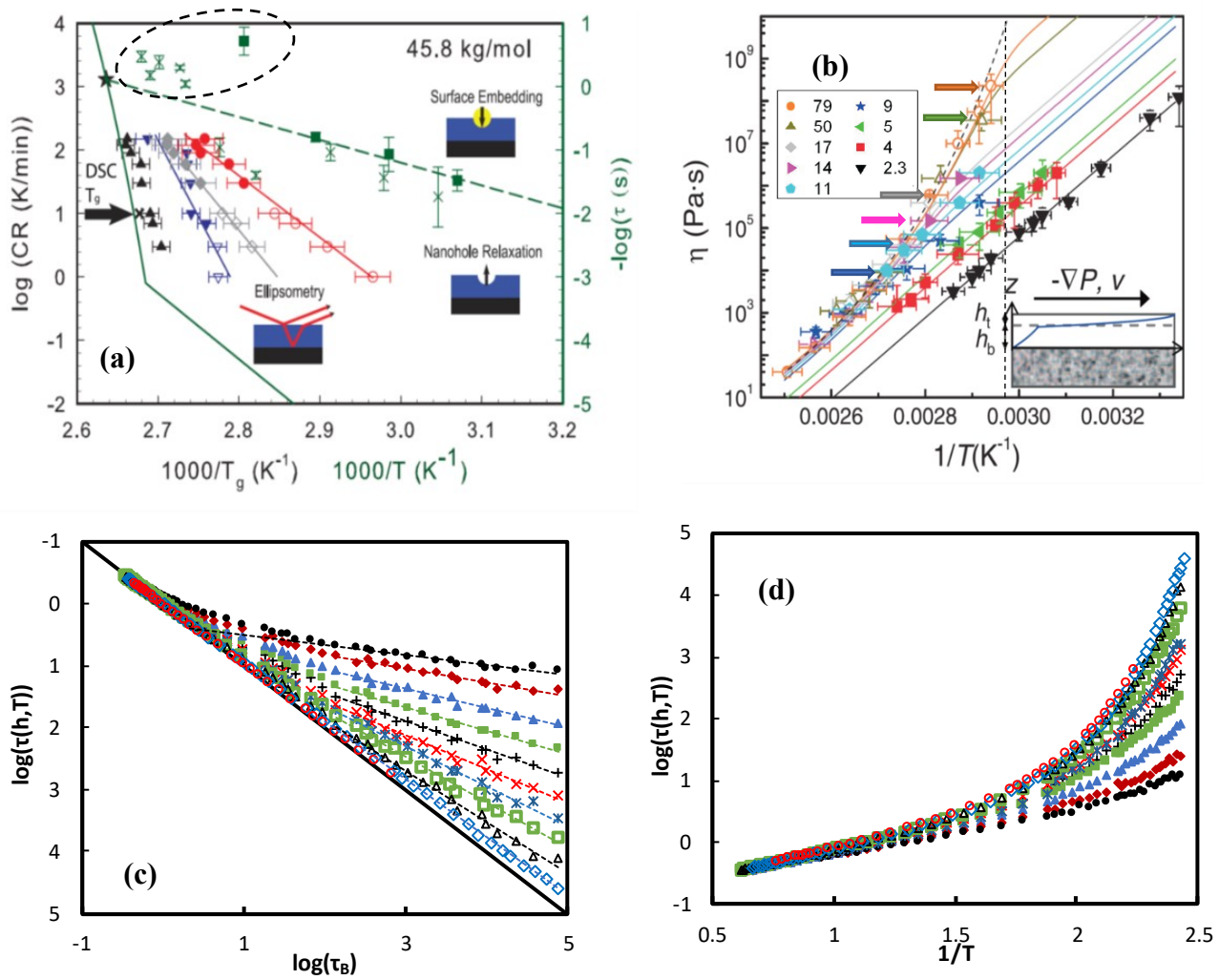

Figure 1. (a) Plot of surface embedding and relaxation rates (green points) vs inverse temperature and cooling rate vs inverse ellipsometric glass transition temperature for films of thickness 274 nm, 34 nm, 18 nm, and 8 nm from bottom to top (other data sets), reproduced with permission from reference 46. The dashes oval is added to highlight surface relaxation points suggesting a higher-temperature actual onset for dynamic very near the surface. (b) Plot of film viscosity vs inverse temperature for films of decreasing thickness (with thickness in nm noted in the inset) from top to bottom, adapted with permission from reference 47. As a guide to the eye, horizontal arrows in corresponding coloring have been added to the original plot to identify the approximate location where near-bulk response is recovered on heating for each film thickness. A dashed vertical line has also been added to denote the reported bulk T_g of the polymer. (c) Film-average translational relaxation time plotted versus bulk translational relaxation time and (d) film-averaged translational relaxation time plotted vs inverse temperature for films of thickness, in units of σ (from top to bottom in part c and bottom to top in part d) 4.2 (black filled circles), 5.1 (red filled diamonds), 6.5 (blue filled triangles), 7.9 (green filled squares), 9.6 (black plusses), 12.0 (red x's), 14.5 (blue stars), 18.2 (green open squares), 26.2 (black open triangles), 47.4 (blue open diamonds), and 93.0 (red open circles). The solid line in part c represents the bulk behavior. Dashed lines in part c are linear fits to each data set over the range 2 to 5.

There are several differences in this onset relative to the ellipsometry results of Fakhraai and coworkers. Specifically, in Fakhraai and coworkers' case, the onset was observed to be roughly thickness independent, while the activation energy of an empirical Arrhenius fit at lower temperatures was found to be thickness-dependent. In contrast, Tsui and coworkers' data exhibits a trend towards higher onset temperatures for thinner films, with the onset temperature diverging (effectively

disappearing) for the thinnest films where $h \leq 5$ nm. It is possible that this represents a qualitative difference between the onset behavior in ellipsometry and viscometry (sharp vs diffuse). However, we note first that the literal disappearance of the onset is only observed in the rheometry at thicknesses $h \leq 5$ nm, which is thinner than the thinnest film probed by Fakhraai and coworkers in the data set shown in Figure 1a[46]. Furthermore, as noted above, the nanohole relaxation data in particular, which probe near surface relaxation in Fakhraai's systems, suggest the possibility that the near-surface onset may be at located considerably higher temperatures / shorter times, which one would expect to be reflected in very thin film dynamics. It is thus quite plausible that ellipsometric measurements might reveal a diverging onset temperature for considerably thinner films. Further ellipsometric measurements in ultrathin films would be helpful in resolving this question, but such measurements are exceedingly difficult.

Second, we emphasize that it is not possible to treat Tsui and coworkers' data via Fakhraai's Arrhenius extrapolation, because the data do not extend to temperatures sufficiently far below the onset to allow a meaningful fit in this regime. As shown in Figure 1b, Tsui and coworkers hypothesized a return to Arrhenius dynamics with a thickness-invariant activation barrier for temperatures well below the (thickness dependent) onset. If true, this would contrast with Fakhraai and coworkers' observed thickness-dependent activation barrier. In practice, however, Tsui and coworkers' data do not extend to low enough temperatures to draw any firm conclusions regarding this regime for films of thickness greater than 5 nm. In summary, the differing temperature regimes probed by the two studies require two distinct approaches to assessing the onset: in Fakhraai and coworkers' work, via extrapolation; in Tsui and coworkers' work, via direct observation without access to lower-T data.

Despite these methodological differences, however, a central element of the phenomenology is quite clear from these two studies. In both cases, for any given film of thickness $h > 5$ nm, measurements identify an onset temperature above which (relaxation time below which) alterations in dynamics are muted or absent. While this onset condition has often been assumed to be fairly fixed across systems and measurements, a comparison of these two data sets (performed for the first time in a recent review article by one of us[1]) suggest that it in fact possesses substantial sensitivities to relaxation function and/or chemistry[1].

Specifically, there appears to be a multiple order of magnitude difference in the onset timescale of strong interfacial effects on dynamics in low molecular weight polystyrene (PS) as measured by Fakhraai's ellipsometry experiments[46] vs Tsui's nanorheometry experiment[47]. The cooling-rate-resolved ellipsometry measurements by Fakhraai and coworkers shown in Figure 1a place the onset temperature for a low-molecular-weight polystyrene (PS) only several Kelvin above T_g[46], corresponding to a relaxation timescale ~100 times shorter than that associated with T_g. Using the standard 100 s relaxation time convention for T_g, this suggests an onset timescale of ~1 s, for films extending down to 8 nm in thickness. In contrast,

the rheological measurements by Tsui and coworkers indicate that substantial alterations in dynamics for thin films of low molecular weight PS persist to approximately 40 K above T_g (Figure 1b).[47] Tsui and coworkers report a bulk T_g of 337 ± 2 K at the molecular weight they employ. Applying this T_g to the bulk dynamics curve shown in Figure 1b suggests a viscosity of ~10^{10} Pa s at this polymer's T_g. For the 9 nm film – the thinnest film for which a clear return to bulk is observed on heating, and a film comparable to the thinnest (8 nm) film probed by Fakhraai and coworkers in Figure 1a – the onset condition appears to be at a viscosity of 10^3 – 10^4 Pa s. The onset condition observed in viscous response thus appears to be 6-7 decades in timescale shorter than that associated with T_g. Again employing the 100 s convention for the relaxation time at T_g to convert to equivalent time units, this suggests that the relaxation time at the rheological onset is 10 μs to 100 μs. *These results point to an onset timescale observed in Tsui's polystyrene viscous response data that is 4-5 orders of magnitude earlier in time that that for Fakhraai's polystyrene ellipsometry data.*

To what factors should we attribute this difference in onset timescale of strong nanoconfinement effects in the same underlying polymer? One might initially attribute this difference to a difference in molecular weight: Tsui's study employed a lower molecular weight (2.4 kg/mol) than did Fakhraai's study (45.8 kg/mol). Evidence from simulations and experiments suggests that the strength of T_g shifts in thin films can be molecular weight dependent in some cases but not others[48], and it is certainly conceivable that this might result from a molecular weight dependence of the onset. On the other hand, Fakhraai and coworkers have separately measured ellipsometric onset temperatures in *small molecule* systems and in high molecular weight (2,240 kg/mol) polystyrene and in both cases also found an onset in the rough vicinity of 1 s [42,44] – an onset time comparable to their 45.8 kg/mol polystyrene. While this cannot fully exclude a role for molecular weight in the different onset timescales of Tsui and Fakhraai, in our view this combination of studies by Fakhraai and coworkers suggests that the onset timescale of strong ellipsometric nanoconfinement effects is not very molecular weight dependent over the range spanning from small molecules to high molecular weight polymers. If so, this would suggest that the 4-5 order of magnitude difference between the onset timescales observed by Fakhraai and Tsui is at least in large part a consequence of the difference in metrology employed, with the former effectively measuring dilatometric relaxation and the latter measuring viscous relaxation.

More broadly, regardless of the extent to which this difference should be attributed to M_w vs metrology differences, this comparison suggests that variation in this onset could potentially explain a great deal of system-to-system and measurement-to-measurement variation in the apparent strength of alterations in near-interface dynamics when measured at a fixed conventional timescale or cooling rate. Additional experimental data bearing on the molecular weight dependence of these differences would be extremely valuable.

A potentially parallel onset condition has been observed in simulation for the first time in our recent work[49], albeit at even shorter time scales. Specifically, we recently reported that near-interface translational dynamics *at low temperature* obey a fractional power-law decoupling relation with bulk dynamics,

$$\frac{\tau(T,z)}{\tau_B(T)} \propto \left(\frac{\tau_B(T)}{\tau^*(z)} \right)^{-\varepsilon(z)} \quad ,(1)$$

where $\tau(T,z)$ is the relaxation time of a slab of material at distance z from an interface, τ_B is the relaxation time of the material in a bulk state, and $\varepsilon(z)$ is called the "decoupling exponent" and quantifies the fractional reduction in activation barrier, relative to bulk, at a distance z from the interface. Crucially, here τ^* *is an onset timescale of this decoupling phenomenon, obtained by upward extrapolation to the bulk of local dynamics, in a manner parallel to that employed by Fakhraai and coworkers in their ellipsometry experiments.*

Notably, this relation was also found to obtain at the level of the whole film[49], with the dependence on position z in equation (1) simply replaced by a dependence on film thickness h.

$$\frac{\tau(T,h)}{\tau_B(T)} \propto \left(\frac{\tau_B(T)}{\tau^*(h)} \right)^{-\varepsilon(h)} \quad (2)$$

Combining these findings with the experimental findings above suggests that the onset condition may depend strongly on relaxation function probed and on chemistry: ellipsometric measurements apparently tend to report an onset near a 1 s relaxation time; linear rheological experiments tend to report an onset at times ~ 4-5 decades shorter than ellipsometry experiments, and simulations of segmental-scale translational relaxation in a flexible bead-spring polymer report an onset in the range of 1-100 ps (LJ time units). This dependence might account for multiple observations in the field: measurement-to-measurement variation in the strength of nanoconfinement effects; the 'anomalous' finding of strong nanoconfinement effects in some simulations at much higher temperatures and shorter timescales than they are observed in experiment; and the observed chemistry dependence of nanoconfinement 'strength'.

We therefore take as an operating hypothesis the proposition that the onset condition of strong interface effects on dynamics is shifted to even shorter timescales in typical bead-based simulations than in rheological experiments, and that the computational-timescale phenomenon indeed corresponds to the onsets observed at longer timescales in experiment. This seems especially plausible given that the onset timescale inferred from the work of Tsui and coworkers[46] approaches the longest timescales accessible to simulation. Moreover, given that bead simulations and experiments generally exhibit

interfacial alterations in the glass transition of a similar magnitude[1] despite their dramatic differences in timescale, a simple difference in the onset timescale in bead simulations vs experiment would provide a parsimonious explanation for this seeming discrepancy. With this hypothesis in mind, we ask the following questions:

1) Does the onset observed in simulation genuinely correspond with the experimentally observed onsets?
2) Is there an appreciable chemical and/or relaxation function dependence of the onset timescale of strong nanoconfinement effects observed in simulation?
3) If so, do these variations trend in a manner that would rationalize the differences in onset timescale observed between bead-based simulations and experiment?
4) Can these variations in the onset condition rationalize differences in the 'strength' of nanoconfinement effects on the glass transition with chemistry and metrology?
5) What is the fundamental underlying origin of this onset condition?

Here we aim to answer these questions specifically in the context of freestanding films. To do so, we perform molecular dynamics simulations of freestanding thin films comprised of variations of a bead-spring polymer. From a chemical standpoint, we directly probe the effect of chain stiffness, which has been shown to play an important role in modulating thin film "nanoconfinement" effects on T_g[19,21]. Further below, we suggest that insights from these stiffness-based suggested predictions for behavior over a larger range of chemical variations that can be tested in future work. We additionally probe the choice of translational vs reorientational relaxation function to assess the role of metrology.

Results suggest that the onset timescale observed in simulation likely corresponds to the experimental phenomenon. Moreover, we find that this onset depends strongly on chain stiffness and relaxation function. Results further suggest that this onset can be explained by a crossover between dominance of a high-temperature, surface-insensitive activation barrier, and a low-temperature, surface-sensitive barrier. In particular, we find that reduced high-temperature activation barriers correlate with lower onset timescales (higher onset temperatures) of strong nanoconfinement effects. While the focus here in terms of chemistry is on chain stiffness, these findings suggest that that trends in the onset timescale with more diverse chemical variables should be governed by changes in the crossover from dominance of this high-temperature to low-temperature barrier. These shifts can in turn be interpreted in terms of chemistry-related changes in the high-temperature activation barrier and the temperature-dependence of the emergent, glassy low-temperature activation barrier.

This finding further supports the proposition that the onset behavior observed in simulation is essentially equivalent to the onset observed in experiment, by providing a simple explanation for the difference in their timescales. Specifically, coarse-

graining to a bead level (particularly in flexible-chain models) dramatically reduces high-temperature activation barriers, which our results suggest should greatly raise the onset temperature of these effects. Moreover, these results can rationalize large metrological differences in this onset condition based on a metrology-dependence of the crossover in dominance from high- to low-T barriers, potentially explaining apparent inconsistencies in experimental observations of this onset.

Simulation methods

Simulations employ an extension of the attractive version of the bead-spring model of Kremer and Grest[50]. Within our model, each polymer chain consists of 20 beads, with covalently adjacent beads held together by anharmonic bonds given by the finitely extensible nonlinear harmonic (FENE) form

$$E_{FENE} = -0.5K_{bond}R_0^2 \ln\left[1-\left(\frac{r}{R_0}\right)^2\right] + 4\varepsilon_{bond}\left[\left(\frac{\sigma_{bond}}{r}\right)^{12}-\left(\frac{\sigma_{bond}}{r}\right)^{6}\right]+\varepsilon_{bond}, \quad (3)$$

where K_{bond} = 30 is an inelastic spring constant, R_0 = 1.3 is a maximum bond length, ε_{bond} = 0.8 sets the energy scale of the repulsive portion of the bond, σ_{bond} = 1.0 sets the range of this repulsive interaction, and where the second term is truncated at its minimum. This forcefield is similar to a family of bond models that have been shown to yield enhanced resistance to crystallization in thin films[51] without substantially perturbing glass-formation behavior relative to the standard Kremer-Grest model[20], and we have previously employed it in studying interfacial effects on dynamics and glass formation[49]. Non-bonded beads interact via a 12-6 Lennard-Jones (LJ) potential,

$$E_{ij} = 4\varepsilon_{ij}\left[\left(\frac{\sigma_{ij}}{r}\right)^{12}-\left(\frac{\sigma_{ij}}{r}\right)^{6}\right] \quad r < r_{cut}, \quad (4)$$

with interaction strength parameter ε = 1, size parameter σ = 1, and cutoff distance r_{cut} = 2.5. Consistent with prior work probing chain stiffness effects in this class of model[19,52,53], we introduce a cosine bending potential,

$$E = K_{bend}\left[1+\cos(\theta)\right], \quad (5)$$

with the spring constant K_{bend} setting the stiffness of the backbone. We specifically consider the behavior of bead-spring polymers with K_{bend} = 0.0, 0.5, 1.0, and 1.5, in order of increasing stiffness. As shown in prior works[19,52], tuning this bending constant increases the Kuhn length of the chain . For this range of bending constants, chains are still in the relatively flexible regime as compared to other similar works [20,53,54], with our prior work pointing to an increase in the Kuhn length by at most

a factor of 2 over this range[52]. The chains thus are nowhere near the rodlike limit, and pronounced changes in local segmental packing are not expected in this range.

We report results in reduced Lennard Jones units, where the LJ unit of length $\sigma_{LJ} \cong 0.5$ to 2.0 nm[55–57] and the LJ unit of time $\tau_{LJ} \cong 1$ ps. While there is no 'standard' temperature mapping for LJ units, a mapping of 1 LJ temperature unit to 1000 K yields a reasonable qualitative basis for comparison for many purposes, yielding a 100-second-timescale T_g similar to that of high-molecular-weight polystyrene.

We perform simulations using the LAMMPS[58] molecular dynamics package. Simulations in the bulk are performed at a constant pressure P = 0. Freestanding film simulations are nominally performed at constant volume, but the presence of free surfaces yields an effective constant pressure P = 0 ensemble. We employ a Nose-Hoover thermostat, as implemented in LAMMPS with a damping parameter of 2 τ_{LJ}, for temperature control. Bulk simulations employ the Nose-Hoover barostat with a damping parameter of 2 τ_{LJ} and a pressure P = 0. Simulations employ the Verlet time-integrator, with a time step of 0.005 τ_{LJ}. They employ periodic boundary conditions for both freestanding film and reference bulk simulations; films are simulated by including void space above and below the film. In our present simulations. Systems are simulated over a range of thicknesses from 4.2 to 26 σ_{LJ}, and we also employ data from simulations published in our prior paper for films of 47 σ_{LJ} and 96 σ_{LJ} (where in all cases the thickness is reported at $T = 0.5$). Those earlier simulations employed the same simulation and analysis protocol described here. In all simulations the lateral film dimension is at least comparable to the film thickness to prevent lateral finite size effects. The full set of the film thicknesses, corresponding numbers of beads, and cross-sectional dimensions for flexible-polymer simulations is shown in Table 1. Simulations at multiple film thicknesses, discussed above, employ the same number of beads and cross-sectional area as the 15 σ_{LJ} film.

Table 1. Thickness, bead counts, and cross-sectional areas of flexibe-polymer films included in this study. Thickness is reported at a reduced temperature of 0.5.

Film Thickness / σ_{LJ}	Beads	Cross-section / σ_{LJ}
4.2	1740	20 x 20
5.1	2120	20 x 20
6.5	2720	20 x 20
7.9	3320	20 x 20
9.6	4000	20 x 20
12	5000	20 x 20
15	10000	26 x 26
18	10000	23 x 23
26	20000	27 x 27
47	128000	51 x 51
93	1024000	103 x 103

Dynamic data are collected from in-equilibrium configurations obtained via the PreSQ automated quench-and-anneal algorithm described in our group's recent publication[59] and employed in a number of recent works[49,60–62]. We summarize the details of this procedure here. Initial random configurations are annealed into equilibrium during a long isothermal annealing period of 5000 τ_{LJ} at a high temperature. These configurations are then subject to a temperature quench at a rate of 10^{-4} T/τ_{LJ}, with configurations saved at temperatures iteratively chosen by an automated algorithm in an effort to yield approximately even spacing in bulk relaxation time. Each configuration is then subject to an additional isothermal annealing period of duration at least ten times the segmental relaxation time at that temperature. Data are collected from additional runs of duration approximately ten times the relaxation time in order to yield good sampling statistics.

Translational segmental relaxation is quantified via the self-part of the intermediate scattering function:

$$F_s(\boldsymbol{q},t) = \frac{1}{N}\sum_{j}^{N}\left\langle \exp\left[-i\boldsymbol{q}\cdot\left(\boldsymbol{r}_j(t)-\boldsymbol{r}_j(0)\right)\right]\right\rangle \quad (6)$$

where $\boldsymbol{q}$ is the wavevector, $\boldsymbol{r}_i$ is the position of segment i, and t is time. In our implementation, we compute the value of this quantity for many wave vectors corresponding, to within the grid resolution of an inverse space gridding, to a given wavenumber q. We employ q = 7.07, which is comparable to the first peak of the structure factor. We then define the relaxation time as the time at which this function decays to 0.2, employing a Kohlsrauch-Williams-Watts form[63,64] for smoothing and interpolation (but never for extrapolation). This set of conventions is a standard approach for obtaining segmental-scale translational relaxation times from simulation[25,60,61,65–67]. The resulting quantity is closely connected to

results from incoherent neutron scattering experiments. A subscript of "t" is employed in figures to denote dynamical quantities obtained via this relaxation function.

We quantify reorientational relaxation via the reorientational autocorrelation function,

$$C_2(t) = \left\langle P_2\left[\boldsymbol{e}_i(0)\cdot\boldsymbol{e}_i(t)\right]\right\rangle \quad (7)$$

where $\boldsymbol{e}_i(t)$ is the unit vector at time t along bond i and $P_2(\mathrm{x})$ is the second Legendre polynomial of x. This relaxation function is closely connected to the results of dynamical light scattering experiments and is expected to behave in a similar manner as the first Legendre polynomial vector autocorrelation function, which is closely connected to dielectric relaxation. Reorientational relaxation times are then extracted from this in the same manner as for translational relaxation. A subscript of "r" is employed in figures to denote dynamical quantities obtained via this relaxation function.

We note that, as a mathematical matter, the radially averaged self-part of the intermediate scattering function is purely translational (due to radial averaging out of any orientational information), whereas the reorientational function is purely reorientational (since it encodes only information on bond orientation). However, there is certainly a coupling between translational and reorientational processes at a *physical* level; i.e. rotation of a dimer involves both reorientation of its central bonds and translation of its constituent monomers. The question of the extent to which this physical coupling is altered by interfaces is naturally implicated in decoupling between these relaxation processes in the bulk and in thin films, as discussed below.

Results

Comparison of computational and experimental onsets

Whole-film translational relaxation time data vs inverse temperature for these films are shown in Figure 1d. As shown by this figure, these data appear to be in qualitative accord with the experimental thin film rheology data of Tsui et al.[45]: both exhibit the onset behavior discussed above; in both cases thinner films exhibit a higher-temperature onset than thicker films; in both cases dynamics transition from highly super-Arrhenius for bulk and thick films to Arrhenius for very thin films. These correspondences suggest a physical equivalence between the onset we observe in simulation and that observed in Tsui and coworkers' data.

Direct comparison to the data of Fakhraai and coworkers is not possible because their system exhibits essentially Arrhenius dynamics to within uncertainty (including for the thickest films), whereas dynamics in our system are highly non-Arrhenius except for the thinnest films. However, because their data are Arrhenius, i.e.

$$\ln\left(\tau/\tau_0\right) \cong -\Delta E/kT \text{ ,(8)}$$

it follows that a plot of their data vs bulk (or thick film) relaxation time rather than vs inverse temperature would yield qualitatively the same plot, with at most a rescaling of the x-axis. It follows that our data can be compared to theirs by replotting our data as log(τ) vs log(τ_{bulk}). As can be seen in Figure 1c, the results of this procedure are in qualitative agreement with the data of Fakhraai and coworkers. In both cases data at low temperatures (large bulk relaxation times) is linear, with an upwards extrapolation of this low-temperature regime to higher temperatures (lower relaxation times) indicating a return to bulk-like behavior at an onset condition τ^* or T^*.

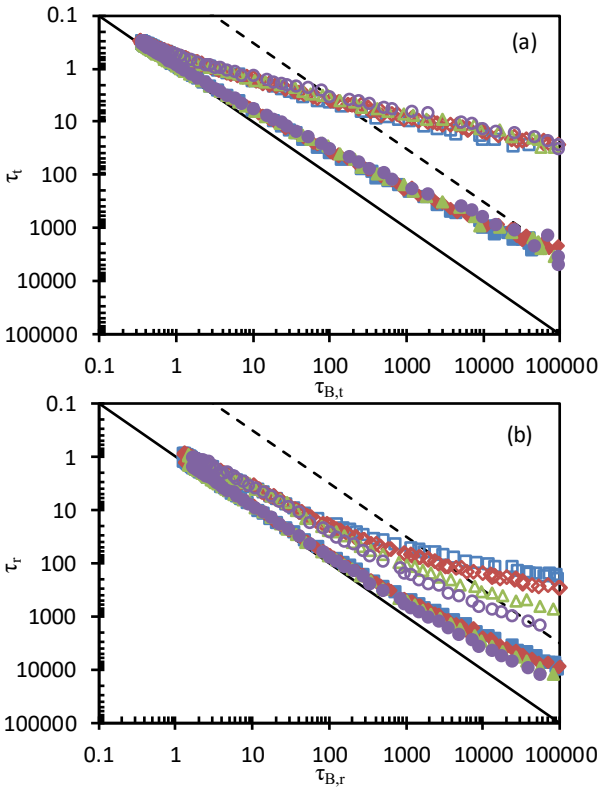

Figure 2. (a) Film (full symbols) and interface layer (hollow symbols) translational relaxation time plotted vs bulk relaxation time for K_θ equal to 0 (blue squares), 0.5 (red diamonds), 1.0 (green triangles), and 1.5 (purple circles). (b) same as (a) for reorientational dynamics. Solid lines represent the bulk relaxation time τ_B. Dashed lines represent $10^{-1.5}\tau_B$; when performing linear fits of the surface layer to equation (1), we include only data further from the bulk than this line.

These results suggest that the onset in simulation indeed corresponds to that observed in rheology and ellipsometry experiments. The combination of this finding with those of Tsui and Fakhkraai suggest that the onset timescale for strong nanoconfinement effects can vary by ~12 orders of magnitude in time (~1 s for ellipsometry on PS and other systems, ~10 μs for rheometry of PS, 1-10 ps for translational relaxation in the bead-spring polymer) as a function of metrology and, perhaps, chemistry. This onset has potentially large implications for interpretation of the apparent magnitude of interface effects on dynamics as probed by different methods. For example, the comparison of Fakhraai's with Tsui's data indicates that, for PS, a rheological measurement might report strong nanoconfinement effects at temperatures for which ellipsometric measurements would find none at all. This onset may also provide important insights into the underlying nature of these effects. Understanding its nature and dependence on chemistry and relaxation function is evidently of high importance.

Dependence of barrier truncation behavior on relaxation function and chain stiffness

In an effort to understand these issues, we next employ simulations across a range of backbone stiffnesses as a coarse measure of the role of chemistry in determining the onset condition. Inspired by a prior simulation reporting stronger

interface effects as measured by translation than reorientation in a polymer film comprised of semiflexible bead-spring chains[19], we also probe both translational and reorientational relaxation to assess whether the onset condition may depend on this choice of relaxation function. In the interest of computational efficiency, here we focus on trends in onset behavior with stiffness for the 15 σ thick film, which is representative of the lower range of thicknesses probed by most experiments.

As shown in Figure 2, the essential equation (1) phenomenology of the onset of a linear relationship between $\log(\tau/\tau_B)$ and $\log(\tau_B)$ at low temperature holds for both reorientational dynamics and translational dynamics, both at a whole-film level and locally for a layer of thickness 0.875 σ_{LJ} at the free surface of the film. At the same time, it is visually clear from this figure from comparison of data across multiple chain stiffnesses that interfacial alterations of translational dynamics are relatively insensitive to chain stiffness, while reorientational dynamics exhibit a suppression of the nanoconfinement effect on τ with increasing stiffness. For the remainder of this paper, we focus on onset behavior for this surface layer of thickness 0.875 σ_{LJ}. As shown by these figures, the overall effect is sufficiently muted at a whole-film level that determination of clean trends is challenged by signal to noise ratio issues.

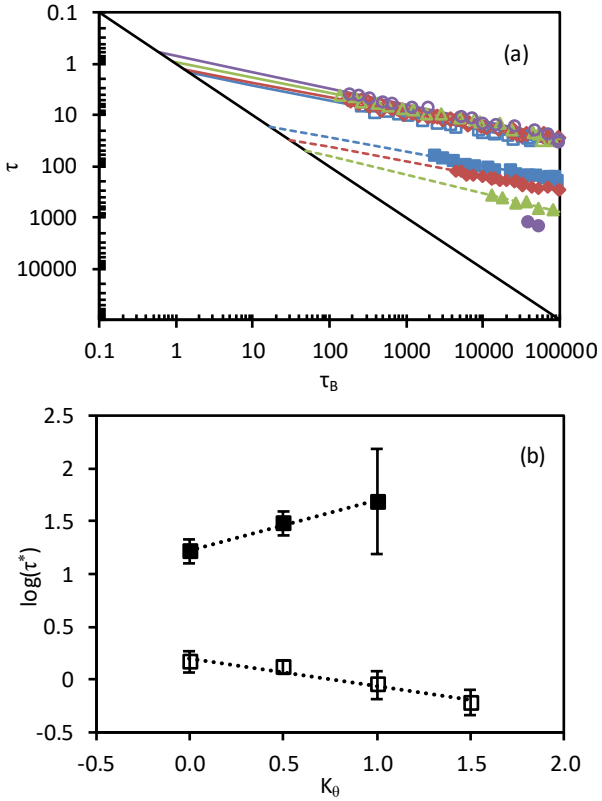

Figure 3. (a) Surface layer relaxation times vs corresponding bulk relaxation times from Figure 2, including only points satisfying the criterion that $\log(\tau/\tau_B) < -1.5$ (corresponding to the dashed line in Figure 2) so as to include only points well beyond the onset. For reorientational relaxation times (filled symbols), the x-axis refers to the bulk reorientational relaxation time; for translational relaxation times (open symbols), the x-axis refers to the bulk translational relaxation time. Dashed and solid lines are fits of these data sets to equation (1) for reorientational and translational dynamics, respectively. The solid black line denotes bulk behavior, with the intersection of each fit curve with the black line corresponding to τ^* for the surface layer in that system. (b) Bulk translational onset timescale τ^*_t for translational decoupling (open symbols) and bulk reorientational onset timescale τ^*_r for reorientational decoupling (filled symbols) as a function of the chain bending constant. Dashed lines in part (b) are linear fits.

There are several ways the one might assess onset behavior based on the data from Figure 2. First, an onset precisely analogous to the procedure employed in experiment by Fakhraai and coworkers by fitting long-time (low temperature data) to the decoupling relation (equation (1)) and extrapolating to lower times / higher temperatures. The onset determined by this method is then the extrapolated bulk relaxation time scale τ^* (or corresponding temperature T^*) at which the low-T film

behavior extrapolates back to bulk. These fits are shown in Figure 3a. In order to ensure that we fit only data that are well past the onset, we restrict the fit to the regime for each data set in which $\log(\tau/\tau_B) < -1.5$, with this criterion illustrated by the dashed lines in Figure 2. We note that this criterion precludes us from performing this analysis for reorientational relaxation for the stiffest chain, which does not include appreciable data in this regime. As shown by Figure 3b, this analysis indicates that the experimentally analogous onset condition τ^* indeed shifts to longer times with higher chain stiffness for reorientation but not for translation. Instead, translational τ^* shift to *shorter* times with increasing stiffness. We include in this figure a linear fit to each of these trends; however, given the uncertainty and range of the data, these fits should be interpreted merely as indicating the sign of the trend and not as compelling evidence for a literal linear dependence on K_θ.

To verify that this finding is not the result of the linear extrapolation performed in Figure 3a, we employ an additional means of quantifying the onset behavior. Specifically, we previously showed[49] that the type of data shown in Figure 2, after normalizing the ordinate by τ_B, can be well-described by a fit to a cosh functional form[68],

$$\log\frac{\tau}{\tau_b} = w\left(\frac{\varepsilon_L-\varepsilon_H}{2}\right)\ln\left(\cosh\frac{\log\left(\tau_b/\tau_{mid}\right)}{w}\right) + \log\left(\tau_b/\tau_{mid}\right)\left(\frac{\varepsilon_L+\varepsilon_H}{2}\right)+\log c \quad (9)$$

where ε_H and ε_L are limiting high and low temperature decoupling exponents, τ_{mid} is the bulk relaxation time at the midpoint of a crossover from the high-T behavior to the well-established low-T fractional power law decoupling regime, w reports on the width of the transition between the two limiting regimes, and $\log c$ is a vertical shift factor. Moreover, differentiating this form then yields a temperature-dependent effective decoupling exponent $\varepsilon(\tau_b)$ through the onset regime.

In our prior paper, we demonstrated that the behavior of $\varepsilon(\tau_b)$ obtained via this treatment is not an artifact of equation (9). We showed, in particular, that the finding of an onset and the low-temperature limiting behavior (which corresponds to the fractional power law decoupling relation) is insensitive to details of the fitting procedure and the choice of other reasonable fitting forms[49]. We do note, however, that for translational dynamics only, the details of the high-temperature behavior and the precise location of the onset *do* depend quantitatively on the treatment of the parameters in equation (9). This results from the fact that, in the flexible bead-spring polymer, the onset condition for translation is found to be fairly near the temperature above which it is not possible to cleanly distinguish the alpha segmental relaxation process from the quasi-ballistic[69] picosecond relaxation. This leads to considerable uncertainty in the high-temperature behavior due to a lack of sufficient data in that regime. As before, here we address this issue by employing an assumption that $\varepsilon_H = 0$ (i.e. return to bulk-like behavior at very high temperatures) for translational relaxation to reduce fit uncertainty that would otherwise result

from the small amount of data available above the onset for this relaxation function. For reorientational relaxation, this issue does not arise because there are sufficient data accessible at temperatures above the onset, and we simply ε_H as a free parameter. Finally, in both cases we constrain *w* to be uniform across the film.

The results of differentiating the equation (9) fits to our τ/τ_B data can be seen in Figure 4. In all cases, the effective temperature-dependent decoupling exponent exhibits a transition from weak or absent decoupling at high temperature to a saturated value at low temperature. The inflection point of this transition, which is the quantity $\log(\tau_{mid})$ in equation (9), can be viewed as an alternate measure of the condition of onset of strong nanoconfinement effects. In terms of the depiction of data shown in Figure 1c and Figure 2, the physical difference between τ^* and τ_{mid} is as follows: τ^* is the point at which an extrapolation of the low-temperature behavior returns to bulk; τ_{mid} reports on the point of maximum curvature in this figure. Were the transition perfectly sharp, the two would be the same; instead generally $\tau^* < \tau_{mid}$, but they are expected to roughly track together.

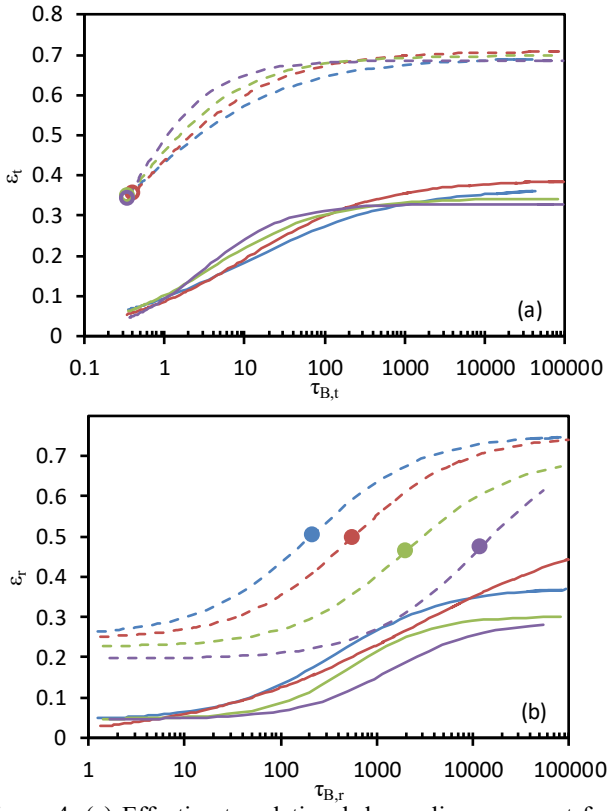

Figure 4. (a) Effective translational decoupling exponent for overall film (solid lines) and interface layer (dashed lines) plotted vs bulk translational relaxation time for several bond angle potentials: $K_\theta = 0.0$ (blue), 0.5 (red), 1.0 (green), and 1.5 (purple). (b) Effective reorientational decoupling exponent for overall film (solid lines) and interface layer (dashed lines) plotted vs bulk reorientational relaxation time, for the same angular potentials shown in part (a). The point on each curve denotes the midpoint for the onset for the dataset in the matching color, where τ_{mid} can be read off as the abscissa value for that point.

The differential analysis in Figure 4 indicates that the onset condition shifts to longer times with increasing chain stiffness for reorientational dynamics; however, no such trend is observed in translation. This can be seen in the midpoint positions shown in this figure: τ_{mid} for reorientational dynamics increases roughly linearly with chain stiffness, while little trend is observed in the translational τ_{mid}. Because the onset of strong reorientational decoupling approaches the upper bound of our simulated time window for the stiffest chains simulated here, the regime of strong reorientational interface effects will move entirely out of the time window of our simulations with appreciable further increases in stiffness. *We thus anticipate that*

higher stiffness chains should exhibit little to no 'nanoconfinement' effect on dynamics and T_g over the range of timescales accessible to simulation.

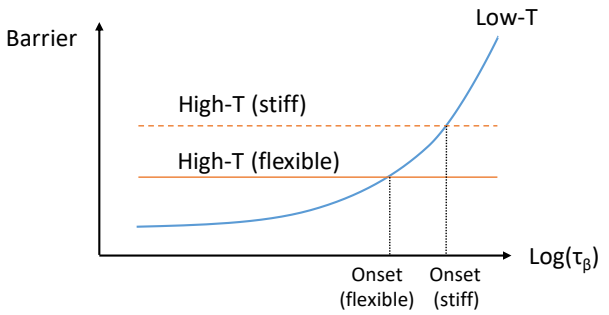

Figure 5. Schematic of two-barrier onset model, illustrating a constant high-T barrier (in orange) and a growing low-T barrier (in blue) vs log bulk relaxation time. The crossover intersection between the two barriers is proposed to drive the onset, with this onset shifting to longer times for systems with a larger high-T barrier, all else being equal.

These results indicate that the onset condition of strong interfacial effects on dynamics is indeed chemistry and metrology dependent, as suggested by comparison of experimental results of Fakhraai and coworkers to those of Tsui and coworkers. In these systems, increasing chain stiffness opens an increasing gap between the onsets of strong interfacial perturbations of translational vs reorientational dynamics. With increasing stiffness, this leads to a situation in which there is some window of temperatures (bulk relaxation times) in which translational dynamics will exhibit a strong perturbation near the interface, but in which reorientaional dynamics exhibit little or no perturbation.

Two-barrier scenario for nanoconfinement effects

These findings raise two central questions. First, what is the origin of the onset of strong decoupling ("strong nanoconfinement effects") at low temperatures observed in simulation and experiment? Second, molecular stiffness alone does not provide a satisfactory predictor of the location of this onset, since it does not explain the difference between this crossover location for translational vs reorientational dynamics within the same system. Can we identify some deeper physics that determine the time scale of this crossover?

We suggest that the onset behavior is parsimoniously predicted at a qualitative level if dynamics in glass-forming liquids are controlled by two distinct barriers:

$$\Delta E(T) = \Delta E_H + \Delta E_L(T) \quad (10)$$

with ΔE_H corresponding to a high-temperature barrier that is at most weakly temperature dependent and a ΔE_L corresponding to a low-temperature barrier that grows much more strongly on cooling. Indeed, a scenario of this kind was suggested by Kivelson et al.[70]. A two-barrier scenario is likewise encoded in the "cooperative" model of Schmidtke et al [71], and a full theoretical prediction of this kind is provided by Mirigian and Schweizer's ECNLE theory[36,72] of supercooled liquid dynamics. Within the latter theory, these two barriers emerge from local caging effects and from longer-range elastic

effects[73], respectively. We note that this 'two barrier' perspective in the glass transition is in contrast to 'single barrier' theories, wherein a single barrier that is present at high-temperature is *amplified* on cooling, typically by an emerging cooperative dynamical length scale. The Adam-Gibbs theory[74] of the glass transition is the canonical example of this single-barrier view point.

If glass formation involves two physically distinct barriers, and if these two barriers have distinct origins, they can be expected to exhibit distinct decoupling exponents, reflecting distinct near-surface truncations relative to bulk:

$$\Delta E(T,z) = \left(1-\varepsilon_H(z)\right)\Delta E_H + \left(1-\varepsilon_L(z)\right)\Delta E_L(T) \quad (11)$$

where $\varepsilon_H(z)$ and $\varepsilon_L(z)$ are high and low temperature decoupling exponents that quantify the position-dependent fractional truncation of the high and low temperature-barriers, respectively. One intuitively expects $\varepsilon_L \gg \varepsilon_H$ under the proposition that more cooperative low-temperature dynamics should be more interface-sensitive than the relatively more local high-temperature dynamics (although this is clearly a heuristic that should be ultimately predicted by a more formal theory of these effects).

If we now consider the effective decoupling exponent accounting for both barriers, we have

$$1-\varepsilon(T,z) = \frac{\Delta E(T,z)}{\Delta E^B(T)} = \frac{\left(1-\varepsilon_H(z)\right)+\left(1-\varepsilon_L(z)\right)\frac{\Delta E_L(T)}{\Delta E_H}}{1+\frac{\Delta E_L(T)}{\Delta E_H}} . \quad (12)$$

It follows that the high and low temperature limits of the decoupling behavior are given by

$$\varepsilon(z) = \begin{cases} \varepsilon_H(z) & \frac{\Delta E_L(T)}{\Delta E_H} \ll 1 \\ \varepsilon_L(z) & \frac{\Delta E_L(T)}{\Delta E_H} \gg 1 \end{cases}, \quad (13)$$

with the crossover temperature T^* between these two regimes then defined by the condition

$$\frac{\Delta E_L(T^*)}{\Delta E_H} = \frac{\Delta E(T^*) - \Delta E_H}{\Delta E_H} = 1 . \quad (14)$$

Equation (14) thus suggests that the onset should be associated with the condition for which the rapidly growing low-temperature barrier first exceeds the relatively constant high temperature barrier. This indicates that, *if the low temperature*

barrier remains relatively unperturbed by a given alteration in chemistry, increases in the high-temperature barrier should delay the onset in decoupling (see schematic representation in Figure 5).

Does this scenario describe the systems simulated here? To test this, for each simulated system we quantify the magnitude of the high-temperature barrier by performing a fit of the high-temperature relaxation regime to an Arrhenius rate law,

$$\tau = \tau_0 \exp\left(\frac{\Delta E_{Arr}}{kT}\right) \quad (15)$$

where ΔE_{Arr} is the high-temperature activation barrier inferred from this fit. There are theoretical reasons to believe that this barrier is likely in fact weakly-temperature dependent[36,72], such that this must be viewed as a leading order approximation reasonable over a limited temperature range.

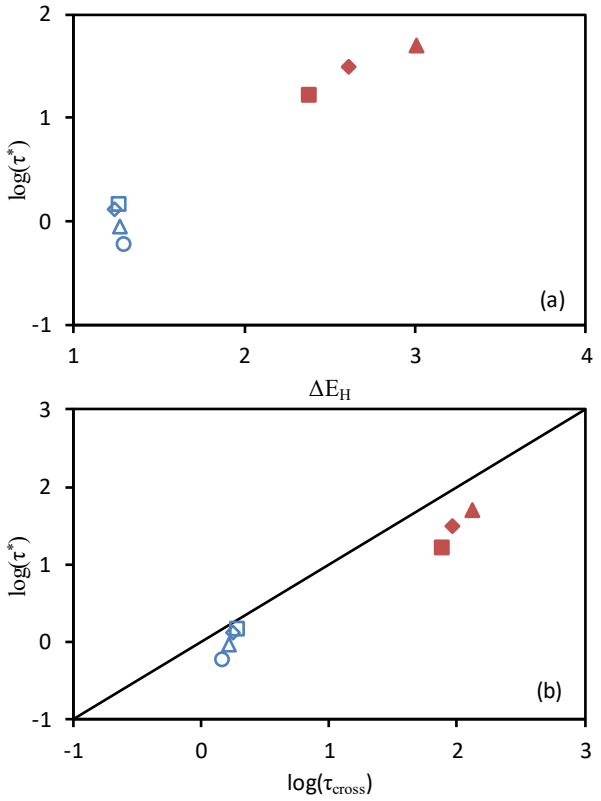

Figure 6. Onset timescale plotted vs (a) the high temperature activation barrier and (b) the approximate crossover timescale at which the low-temperature barrier becomes larger than the high-temperature barrier for reorientational relaxation (red symbols) and translational relaxation (blue symbols) in the bulk. For each relaxation function (translational and reorientational), the onset is in units of the bulk relaxation time for that relaxation function, and bulk activation barriers are likewise computed for the corresponding relaxation function. Symbol *shapes* (but not colors) correspond to those in Figure 2 and Figure 3.

In performing this analysis, we again focus on the onset condition in the surface layer of the film. Our prior results indicated that onset occurs first immediately at the surface[49], and the onset is strongest at this location and thus involves the best signal-to-noise ratio for the purposes of finely detecting trends in the onset condition.

As shown by Figure 6a, the growth in the reorientational decoupling onset timescale τ^* with chain stiffness in these systems corresponds with a growth in the high temperature barrier as chain stiffness increases, with a rough linear relationship observed between onset timescale and high temperature barrier. A similar trend is observed for τ_{mid} (Figure 7a). These results provide an initial indication that the two-barrier model can indeed explain the variation in the onset condition of strong interface effects on both for both translational and reorientational dynamics for these systems.

We can test the two barrier idea even more directly by determining whether the onset timescale of strong nanoconfinement correlates with the timescale of the dominance crossover from the high to low temprerature barrier. To do this, we again determine the high-T barrier based on a fit to the Arrhenius regime. We then determine an effective temperature-dependent

barrier for the bulk system by first fitting the full temperature dependence of the relaxation time to the cooperative model of Schmidtke et al[71]. We then differentiate ln(τ) with respect to inverse temperature in the usual way to arrive at a temperature-dependent effective activation barrier:

$$\Delta E_{eff}(T) = \frac{d \ln \tau}{d(1/kT)} \quad (16)$$

We subtract the (T-invariant) high-T barrier from this total barrier to arrive at an effective low-T barrier. The crossover condition is then the temperature (relaxation time) at which the two barriers are equal. As shown in Figure 6b, the onset timescale τ^* of strong nanoconfinement indeed is very similar to the relaxation timescale at which the low-temperature barrier becomes dominant for all of these systems. A strong linear relationship between τ_{mid} and this crossover condition τ_{cross} is also observed in Figure 7b, albeit with a slope not equal to one. This shift is likely a result of the distinct definitions of τ^* and τ_{mid} noted above. While these correlations are based in a minimal scaling model and are therefore clearly somewhat approximate, these results provide support for the proposition that the onset of 'strong nanoconfinement' is related to the onset of a regime in which a low-temperature barrier becomes dominant.

From a practical standpoint, the results in Figure 6 point to a potential broader interpretation of the trends towards later onsets in stiffer polymers observed above. If the mechanism of this trend is genuinely a shift in the high-temperature barrier, as suggested by Figure 6, then we expect this trend observed in stiffness to be informative of chemical variations more broadly. Specifically, other chemical modifications that tune the relaxation timescale at which the low-T barrier outgrows the high-T barrier should likewise tune the onset condition of strong 'nanoconfinement' effects. Future simulations spanning a broader range of chemistries will be necessary to further test this proposition.

Discussion and Conclusions

These findings point to the following answers to the questions posed in the introduction:

Is there an appreciable chemical and/or relaxation function dependence of the onset timescale of strong nanoconfinement effects observed in simulation?

In both simulations and experiments, the onset condition observed is observed to depend appreciably relaxation function measured. Simulations indicate that the extent of this dependence is additionally dependent on chemistry (as probed here at a coarse level by chain stiffness variations). As discussed further below, the correspondence between the onsets observed in simulation and experiment suggest that similar trends should be observed experimentally, and this would be consistent with

experimental findings pointing towards weaker T_g nanoconfinement effects with increasing stiffness in a homologous series of polymers[21]. Additional experimental observations in this set of systems employing rate scans to probe the experimental stiffness-dependence of the onset condition could be of great value.

What is the underlying origin of this onset condition?

Results suggest that a two-barrier model of glass formation can likely explain the onset in a parsimonious manner, with the onset condition corresponding roughly to a condition at which a low-temperature, interface-sensitive activation barrier becomes dominant over a high-temperature, interface-insensitive barrier. This finding may be related to recent results by Sussman et al., in which a machine learning approach to analysis of local dynamics pointed to the presence of two distinct contributions to dynamics near an interface[75]. The precise relationship between the two barriers posited here and the two contributions reported by Sussman et al. requires further investigation – conceivably they may be closely related. As discussed further below, a physical theory leading to a two-barrier scenario of this kind appears to be potentially provided by the Elastically Cooperative Nonlinear Langevin Equation theory of Mirigian and Schweizer[72,76].

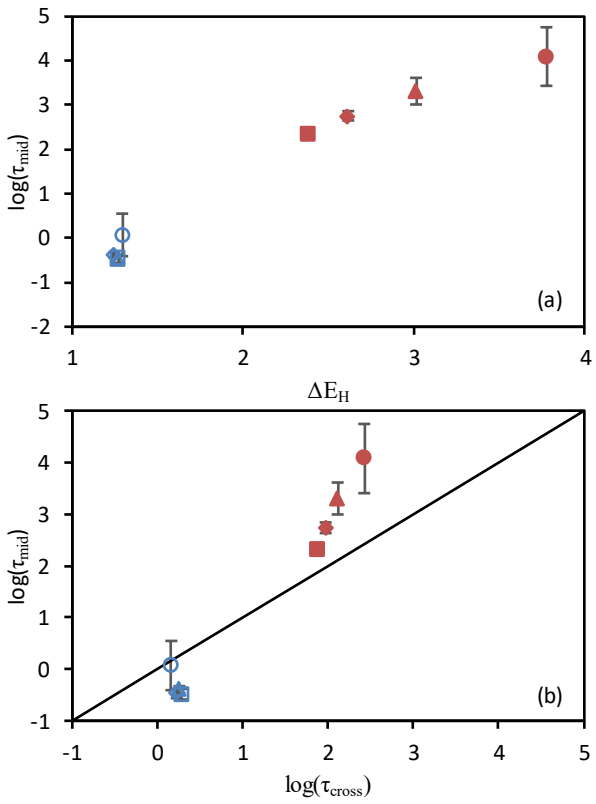

Figure 7. Midpoint timescale plotted vs (a) the high temperature activation barrier and (b) the approximate crossover timescale at which the low-temperature barrier becomes larger than the high-temperature barrier for reorientational relaxation (red symbols) and translational relaxation (blue symbols) in the bulk. For each relaxation function (translational and reorientational), the midpoint is in units of the bulk relaxation time for that relaxation function, and bulk activation barriers are likewise computed for the corresponding relaxation function. Symbol *shapes* (but not colors) correspond to those in Figure 2 and Figure 3. Error bars are 95% confidence intervals from fits to equation (9).

Does the onset observed in simulation genuinely correspond with the experimentally observed onsets? Do variations in the onset timescale trend in a manner that would rationalize the differences in onset timescale observed between bead-based simulations and experiment?

Yes, results suggest that corresponding onset conditions of strong interfacial effects on dynamics are observed, albeit at distinct time scales, in experimental ellipsometry, experimental rheology, simulated translational dynamics, and simulated reorientational dynamics. In particular, the following reasoning points to this correspondence.

1. The onset behavior observed in simulations is qualitatively equivalent to the behavior observed in experiment (compare Figure 1a and Figure 1c), albeit at shorter time scales. For example, Fakhraai's experimental data, with an onset near 1 s, exhibits behavior consistent with the fractional power law decoupling relation (equation (1)) observed with a ps onset timescale in simulations.
2. The difference between the largest simulation onset relaxation timescale and smallest experimental onset relaxation timescale reported or reviewed here is smaller than the variation in onset timescales directly observed within the simulations or experiments themselves. We observe onset timescales (in bulk relaxation time units) as long as ~10 ns in simulation. Associating T_g with a 100-second timescale, Tsui and coworkers' rheological data appear to involve an onset timescale in the range of 10 to 100 μs. The gap between simulation and experiment is thus only 3-4 orders of magnitude. By comparison, direct experimental evidence (i.e. the comparison of Tsui and coworkers' data[47] with Fakhraai and coworkers' data[46]) demonstrates that some combination of chemistry and metrology leads to a 4-5 decade variation in this onset timescale in experiment. Similarly, our simulations exhibit a ~4 decade variation in onset timescale based upon a combination of backbone stiffness and metrology. *Of the overall ~12 decade onset timescale variation from the shortest-onset simulations to the longest-onset experiments, direct evidence from simulations and experiments thus reports on variations over ~2/3 of this range* (see Figure 1 and associated discussion). The remaining timescale difference that must be accounted for between simulations and experiments is thus relatively small.
3. The trend in our simulation data is to later onset times as the high-temperature activation barrier is increased (see Figure 6 and Figure 7), such that that a modest extrapolation would yield values comparable to the shortest-onset-timescale experiments. Both the two-barrier model and the raw data provide an argument that simple-bead-based models should generally yield onset conditions appreciably higher than experiment. Specifically, both indicate that systems with lower high-temperature activation barriers will, all else being equal, exhibit onset conditions of strong nanoconfinement at higher temperatures (shorter relaxation times) than systems with larger high-temperature barriers. One of the central results of coarse-graining is to suppress the high-temperature activation barrier due to smoothing of the potential energy landscape. For this reason, coarse-grained models, and especially the bead-based physics models commonly employed in computational study of glassy dynamics, have high-T barriers that are far lower than their atomistically resolved analogues in all-atom simulation and in experiment. Thus, our results and the two-layer model indicate that these bead

models will naturally have much higher onset temperatures (lower onset times) than chemically realistic systems. Indeed, as recently pointed out in our perspective[1], work by Rossler and coworkers has reported high-temperature barriers in realistic systems that are much larger than those in coarse models[71,77,78], supporting this proposition.

4. Simulations report thin-film T_g perturbations that are comparable in magnitude (when normalized by bulk T_g's) to experiments, despite the large difference in time scales[10,55,79]. This near quantitative correspondence can be explained by the difference in onset timescales proposed here. Specifically, our prior paper[49] and recent perspective[1] derive, via a VFT model, a connection between the decoupling exponent and the glass transition temperature. These relations demonstrate that, for fixed magnitude of decoupling, the apparent T_g shift is a function of the number of decades in relaxation time past the onset of strong nanoconfinement at which T_g is measured. For bead-based flexible polymer simulations, the onset is at 1-100 ps, with many simulation studies involving maximum timescales in the range of 1-100 ns. By comparison, ellipsometric measurements (the most common means of measuring thin film T_g) appear to commonly involve an onset of nanoconfinement effects in the range of 0.1 to 1s, with longest timescales typically in the range of 100 to 1000 s. Both simulation and measurement thus commonly involve timescales in the range of 2-4 orders of magnitude beyond the onset. This fact may explain why simulations so commonly exhibit T_g perturbations in confined systems that are comparable to those in experiment[10,55,79] despite involving vastly shorter timescales.

This reasoning suggests that simulation study of strong interfacial effects on dynamics is possible via a fortuitous cancellation of differences: simulations of bead models access shorter timescales, but involve correspondingly short onset times.

We note that, in addition to bead-spring type models, there exist a set of systematically coarse-grained models that aim to more quantitatively reproduce specific polymeric systems[48,80,81]. These systems would make for an excellent additional test of the mechanism onset mechanism suggested here, which might explain how they can quantitatively reproduce experimental trends despite involving much shorter timescales than experiment. Direct study of onset behavior in these types of simulated systems should be a priority.

Can variations in the onset condition rationalize differences in the 'strength' of nanoconfinement effects on the glass transition with chemistry and metrology?

Broadly, these results indicate that one should generally anticipate differences in the onset timescale of strong nanoconfinement effects when employing distinct metrologies that reflect distinct underlying relaxation functions. Because the extent of T_g perturbations is a function of the degree of supercooling beyond this onset, this indicates that distinct

relaxation functions should be expected to report different T_g alterations. In the extreme case of a measurement made above the onset for one relaxation function but below the onset for another, one may expect to see bulk-like T_g in the first case and strongly perturbed T_g in the second. This is not an experimental anomaly, but rather a reflection of the apparent fact that distinct relaxation functions are subject to distinct perturbations in thin films.

Given that our results *specifically* point to a likelihood of distinct interfacial effects on translational and reorientational relaxation, these findings may have particular relevance to the interpretation of dielectric spectroscopy experiments in thin films. A considerable volume of debate has surrounded the perception that dielectric spectroscopy often reports weaker (or absent) effects of free surfaces on dynamics than do other methods[27]. We have previously shown that differences in the manner by which dynamic and pseudo-thermodynamic measurements weight their respective averages over dynamics gradients may play a role in these differences. The present findings indicate that, moreover, *the underlying dynamical gradient for reorientational relaxation may commonly be weaker, when compared at a fixed observation timescale, than gradients for measures of translational relaxation due a later timescale of onset.* Since dielectric spectroscopy probes reorientational relaxation, it is to be expected the dielectric spectroscopy may commonly report weaker dynamical perturbations when compared at equal relaxation timescale or temperature to other measurements, at least near the free surfaces probed in this study.

These findings may cast new light on efforts to understand differences in the apparent susceptibility of distinct chemistries to interfacial effects on dynamics and glass formation. These findings suggest that, rather than purely a matter of a chemistry-dependent strength, the issue may involve a chemistry-dependent onset. Chemistries in which the low-T barrier comes to dominate at lower temperature will naturally exhibit apparently weaker effects in a fixed-time-window experiment. Because the two-barrier model naturally links this onset to the temperature dependence of dynamics, it may ultimately provide an explanation for the observation the apparent strength of nanoconfinement effects often [16–18], but not always[19–21], correlates with the fragility of glass formation.

These findings may additionally bear on expectations regarding the dependence of nanoconfinement effects on the fragility of glass formation. There is some evidence for a trend towards weaker nanoconfinement effects in less fragile (more Arrhenius) glass formers within at least some well-defined sets of chemistries[18], although this trend may be nonuniversal[20]. In very strong (non-fragile) glass-formers where the origin of non-fragility is a dominance of the high-T barrier over the entire glass formation range, the two-barrier picture for the onset would tend to anticipate considerably attenuated interfacial effects on dynamics. On the other hand, a *universal* trend *quantitatively* relating confinement effect strength to fragility is *not* to be expected from this perspective, because fragility primarily reports on the magnitude of the low-T barrier, whereas

the focus in this picture is on the crossover from high- to low-T barriers. A test of these propositions in future experiments and simulations could be of considerable value.

We further emphasize that these results point to a *combined* effect of metrology and chemistry on the onset timescale. For example, these simulations find no appreciable trend in the onset condition for alterations in *translational* dynamics near interfaces, but an appreciable trend in the onset for *reorientational* dynamics near interfaces. In experiment, ellipsometric experiments by Fakhraai and coworkers in a modest number of chemistries have identified fairly similar onset timescales (at least to within several decades) in supported films[43,44,46,82,83]. This may indicate that the *ellipsometric* onset timescale is relatively chemistry insensitive, although considerably more data is needed to draw this conclusion firmly. The extent to which the onset timescale for other metrologies (such as the rheological experiments of Tsui and coworkers[47] or Priestley and coworkers[84]) depends on chemistry must be explored with new experimental data.

All of these questions are addressed here in the context of freestanding films at low molecular weight. Additional complications may arise in the context of supported films, and further simulation study of onset behavior in that context is needed to connect more quantitatively with experiment. Moreover, there is some evidence of new effects (such as two T_g's) in some very high molecular weight polymer films[82,85]; the present findings cannot provide insight into those effects, and access to these molecular weights will be very challenging given limitations on simulation time scales. We also note that the concept of an onset timescale or return to bulk has, thus far, been considered in experiment and simulation in the context of a *mean* T_g or relaxation time. There is experimental evidence for changes in the *breadth* of the glass transition in thin films[82,86]; the question of whether the onset condition for the mean film behavior also reflects a return to a bulk-like distribution of relaxation times or effective stretching exponent is an open one; we plan to address this question in future work.

Finally, we note that the Elastically Cooperative Nonlinear Langevin Equation theory of glass formation, which explicitly invokes two distinct contributions to the barrier, predicts both temperature-invariant decoupling and the presence of two barriers, making it a promising candidate for description of this behavior[36,72,87]. At present, ECNLE focuses on a single type of relaxation process – translational relaxation. The question of relaxation-function-dependences of the onset therefore is not presently within the scope of this theory. More broadly, most theories of the glass transition in bulk and under nanoconfinement focus only on translational relaxation or on general relaxation, presumably under the working hypothesis that distinct processes track at least roughly together. Given that these findings point to an important role for quantitative differences between translational and reorientational nanoconfinement effects, it is of evident practical importance for future

theoretical efforts in the field to specify the precise relaxation function under consideration and to include predictions for multiple relaxation processes.

Acknowledgments

This material is based upon work supported by the National Science Foundation under Grant No. CBET 1705738. The authors acknowledge the W. M. Keck Foundation for generous support enabling development of simulation methodologies employed in this work. The authors thank K. Schweizer for valuable discussions. The authors thank Z. Fakhraai and R. Riggleman for early discussions that helped motivate this work.

References

(1) Schweizer, K. S.; Simmons, D. S. Progress towards a Phenomenological Picture and Theoretical Understanding of Glassy Dynamics and Vitrification near Interfaces and under Nanoconfinement. *J. Chem. Phys.* **2019**, *151*, 240901.

(2) Keddie, J. L.; Jones, R. A. L.; Cory, R. A. Size-Dependent Depression of the Glass Transition Temperature in Polymer Films. *Europhys. Lett. EPL* **1994**, *27*, 59–64. https://doi.org/10.1209/0295-5075/27/1/011.

(3) Jackson, C. L.; McKenna, G. B. The Glass Transition of Organic Liquids Confined to Small Pores. *J. Non-Cryst. Solids* **1991**, *131–133, Part 1*, 221–224. https://doi.org/10.1016/0022-3093(91)90305-P.

(4) Simmons, D. S. An Emerging Unified View of Dynamic Interphases in Polymers. *Macromol. Chem. Phys.* **2016**, *217* (2), 137–148. https://doi.org/10.1002/macp.201500284.

(5) Ediger, M. D.; Forrest, J. A. Dynamics near Free Surfaces and the Glass Transition in Thin Polymer Films: A View to the Future. *Macromolecules* **2014**, *47* (2), 471–478. https://doi.org/10.1021/ma4017696.

(6) Cangialosi, D.; Boucher, V. M.; Alegria, A.; Colmenero, J. Physical Aging in Polymers and Polymer Nanocomposites: Recent Results and Open Questions. *Soft Matter* **2013**, *9*, 8619–8630. https://doi.org/10.1039/C3SM51077H.

(7) Richert, R. Dynamics of Nanoconfined Supercooled Liquids. *Annu. Rev. Phys. Chem.* **2011**, *62* (1), 65–84. https://doi.org/10.1146/annurev-physchem-032210-103343.

(8) McKenna, G. B. Ten (or More) Years of Dynamics in Confinement: Perspectives for 2010. *Eur. Phys. J. Spec. Top.* **2010**, *189* (1), 285–302. https://doi.org/10.1140/epjst/e2010-01334-8.

(9) Roth, C. B.; Dutcher, J. R. Glass Transition and Chain Mobility in Thin Polymer Films. *J. Electroanal. Chem.* **2005**, *584* (1), 13–22. https://doi.org/10.1016/j.jelechem.2004.03.003.

(10) Napolitano, S.; Glynos, E.; Tito, N. B. Glass Transition of Polymers in Bulk, Confined Geometries, and near Interfaces. *Rep. Prog. Phys.* **2017**, *80* (3), 036602. https://doi.org/10.1088/1361-6633/aa5284.

(11) O'Connell, P. A.; Hutcheson, S. A.; McKenna, G. B. Creep Behavior of Ultra-Thin Polymer Films. *J. Polym. Sci. Part B Polym. Phys.* **2008**, *46* (18), 1952–1965. https://doi.org/10.1002/polb.21531.

(12) O'Connell, P. A.; Wang, J.; Ishola, T. A.; McKenna, G. B. Exceptional Property Changes in Ultrathin Films of Polycarbonate: Glass Temperature, Rubbery Stiffening, and Flow. *Macromolecules* **2012**, *45* (5), 2453–2459. https://doi.org/10.1021/ma300098h.

(13) Merling, W. L.; Mileski, J. B.; Douglas, J. F.; Simmons, D. S. The Glass Transition of a Single Macromolecule. *Macromolecules* **2016**, *49* (19), 7597–7604. https://doi.org/10.1021/acs.macromol.6b01461.

(14) Lang, R. J.; Merling, W. L.; Simmons, D. S. Combined Dependence of Nanoconfined Tg on Interfacial Energy and Softness of Confinement. *ACS Macro Lett.* **2014**, *3*, 758–762. https://doi.org/10.1021/mz500361v.

(15) Fryer, D. S.; Peters, R. D.; Kim, E. J.; Tomaszewski, J. E.; Nealey, P. F.; White, C. C.; Wu, W. L. Dependence of the Glass Transition Temperature of Polymer Films on Interfacial Energy and Thickness. *Macromolecules* **2001**, *34*, 5627.

(16) Delcambre, S. P.; Riggleman, R. A.; de Pablo, J. J.; Nealey, P. F. Mechanical Properties of Antiplasticized Polymer Nanostructures. *Soft Matter* **2010**, *6* (11), 2475–2483. https://doi.org/Article.

(17) Riggleman, R. A.; Yoshimoto, K.; Douglas, J. F.; de Pablo, J. J. Influence of Confinement on the Fragility of Antiplasticized and Pure Polymer Films. *Phys. Rev. Lett.* **2006**, *97* (4), 045502.

(18) Evans, C. M.; Deng, H.; Jager, W. F.; Torkelson, J. M. Fragility Is a Key Parameter in Determining the Magnitude of Tg-Confinement Effects in Polymer Films. *Macromolecules* **2013**, *46* (15), 6091–6103. https://doi.org/10.1021/ma401017n.

(19) Shavit, A.; Riggleman, R. A. Influence of Backbone Rigidity on Nanoscale Confinement Effects in Model Glass-Forming Polymers. *Macromolecules* **2013**, *46*, 5044–5052. https://doi.org/10.1021/ma400210w.

(20) Mangalara, J. H.; Marvin, M. D.; Wiener, N. R.; Mackura, M. E.; Simmons, D. S. Does Fragility of Glass Formation Determine the Strength of Tg-Nanoconfinement Effects? *J. Chem. Phys.* **2017**, *146* (10), 104902. https://doi.org/10.1063/1.4976521.

(21) Torres, J. M.; Wang, C.; Coughlin, E. B.; Bishop, J. P.; Register, R. A.; Riggleman, R. A.; Stafford, C. M.; Vogt, B. D. Influence of Chain Stiffness on Thermal and Mechanical Properties of Polymer Thin Films. *Macromolecules* **2011**, *44* (22), 9040–9045. https://doi.org/10.1021/ma201482b.

(22) Solar, M.; Mapesa, E. U.; Kremer, F.; Binder, K.; Paul, W. The Dielectric Alpha-Relaxation in Polymer Films: A Comparison between Experiments and Atomistic Simulations. *Epl* **2013**, *104* (6), 66004. https://doi.org/10.1209/0295-5075/104/66004.

(23) Ye, C.; Weiner, C. G.; Tyagi, M.; Uhrig, D.; Orski, S. V.; Soles, C. L.; Vogt, B. D.; Simmons, D. S. Understanding the Decreased Segmental Dynamics of Supported Thin Polymer Films Reported by Incoherent Neutron Scattering. *Macromolecules* **2015**, *48* (3), 801–808. https://doi.org/10.1021/ma501780g.

(24) Pye, J. E.; Rohald, K. A.; Baker, E. A.; Roth, C. B. Physical Aging in Ultrathin Polystyrene Films: Evidence of a Gradient in Dynamics at the Free Surface and Its Connection to the Glass Transition Temperature Reductions. *Macromolecules* **2010**, *43* (19), 8296–8303. https://doi.org/10.1021/ma101412r.

(25) Lang, R. J.; Simmons, D. S. Interfacial Dynamic Length Scales in the Glass Transition of a Model Freestanding Polymer Film and Their Connection to Cooperative Motion. *Macromolecules* **2013**, *46* (24), 9818–9825. https://doi.org/10.1021/ma401525q.

(26) Tress, M.; Erber, M.; Mapesa, E. U.; Huth, H.; Müller, J.; Serghei, A.; Schick, C.; Eichhorn, K.-J.; Voit, B.; Kremer, F. Glassy Dynamics and Glass Transition in Nanometric Thin Layers of Polystyrene. *Macromolecules* **2010**, *43* (23), 9937–9944. https://doi.org/10.1021/ma102031k.

(27) Kremer, F.; Tress, M.; Mapesa, E. U. Glassy Dynamics and Glass Transition in Nanometric Layers and Films: A Silver Lining on the Horizon. *J. Non-Cryst. Solids* **2015**, *407*, 277–283. https://doi.org/10.1016/j.jnoncrysol.2014.08.016.

(28) Erber, M.; Tress, M.; Mapesa, E. U.; Serghei, A.; Eichhorn, K.-J.; Voit, B.; Kremer, F. Glassy Dynamics and Glass Transition in Thin Polymer Layers of PMMA Deposited on Different Substrates. *Macromolecules* **2010**, *43* (18), 7729–7733. https://doi.org/10.1021/ma100912r.

(29) Serghei, A.; Huth, H.; Schick, C.; Kremer, F. Glassy Dynamics in Thin Polymer Layers Having a Free Upper Interface. *Macromolecules* **2008**, *41* (10), 3636–3639. https://doi.org/10.1021/ma702381t.

(30) Serghei, A.; Kremer, F. Broadband Dielectric Spectroscopy on Ultrathin Organic Layers Having One Free (Upper) Interface. *Rev. Sci. Instrum.* **2006**, *77* (11), 116108. https://doi.org/10.1063/1.2372740.

(31) Forrest, J. A. What Can We Learn about a Dynamical Length Scale in Glasses from Measurements of Surface Mobility? *J. Chem. Phys.* **2013**, *139* (8), 084702.

(32) Forrest, J. A.; Dalnoki-Veress, K. When Does a Glass Transition Temperature Not Signify a Glass Transition? *ACS Macro Lett.* **2014**, *3*, 310–314. https://doi.org/10.1021/mz4006217.

(33) Kim, S.; Hewlett, S. A.; Roth, C. B.; Torkelson, J. M. Confinement Effects on Glass Transition Temperature, Transition Breadth, and Expansivity: Comparison of Ellipsometry and Fluorescence Measurements on Polystyrene Films. *Eur. Phys. J. E* **2009**, *30* (1), 83–92. https://doi.org/10.1140/epje/i2009-10510-y.

(34) Mangalara, J. H.; Mackura, M. E.; Marvin, M. D.; Simmons, D. S. The Relationship between Dynamic and Pseudo-Thermodynamic Measures of the Glass Transition Temperature in Nanostructured Materials. *J. Chem. Phys.* **2017**, *146* (20), 203316. https://doi.org/10.1063/1.4977520.

(35) Marvin, M. D.; Lang, R. J.; Simmons, D. S. Nanoconfinement Effects on the Fragility of Glass Formation of a Model Freestanding Polymer Film. *Soft Matter* **2014**, *10* (18), 3166–3170. https://doi.org/10.1039/C3SM53160K.

(36) Mirigian, S.; Schweizer, K. S. Communication: Slow Relaxation, Spatial Mobility Gradients, and Vitrification in Confined Films. *J. Chem. Phys.* **2014**, *141* (16), 161103. https://doi.org/10.1063/1.4900507.

(37) Lipson, J. E. G.; Milner, S. T. Percolation Model of Interfacial Effects in Polymeric Glasses. *Eur. Phys. J. B* **2009**, *72* (1), 133–137. https://doi.org/10.1140/epjb/e2009-00324-y.

(38) Rotella, C.; Wübbenhorst, M.; Napolitano, S. Probing Interfacial Mobility Profiles via the Impact of Nanoscopic Confinement on the Strength of the Dynamic Glass Transition. *Soft Matter* **2011**, *7* (11), 5260–5266. https://doi.org/10.1039/C1SM05430A.

(39) Mirigian, S.; Schweizer, K. S. Theory of Activated Glassy Relaxation, Mobility Gradients, Surface Diffusion, and Vitrification in Free Standing Thin Films. *J. Chem. Phys.* **2015**, *143* (24), 244705. https://doi.org/10.1063/1.4937953.

(40) Lipson, J. E. G.; Milner, S. T. Local and Average Glass Transitions in Polymer Thin Films. *Macromolecules* **2010**, *43* (23), 9874–9880. https://doi.org/10.1021/ma101099n.

(41) Fakhraai, Z.; Forrest, J. A. Probing Slow Dynamics in Supported Thin Polymer Films. *Phys. Rev. Lett.* **2005**, *95* (2), 025701. https://doi.org/10.1103/PhysRevLett.95.025701.

(42) Daley, C. R.; Fakhraai, Z.; Ediger, M. D.; Forrest, J. A. Comparing Surface and Bulk Flow of a Molecular Glass Former. *Soft Matter* **2012**, *8* (7), 2206–2212. https://doi.org/10.1039/C2SM06826E.

(43) Glor, E. C.; Composto, R. J.; Fakhraai, Z. Glass Transition Dynamics and Fragility of Ultrathin Miscible Polymer Blend Films. *Macromolecules* **2015**, *48* (18), 6682–6689. https://doi.org/10.1021/acs.macromol.5b00979.

(44) Zhang, Y.; Glor, E. C.; Li, M.; Liu, T.; Wahid, K.; Zhang, W.; Riggleman, R. A.; Fakhraai, Z. Long-Range Correlated Dynamics in Ultra-Thin Molecular Glass Films. *J. Chem. Phys.* **2016**, *145* (11), 114502. https://doi.org/10.1063/1.4962734.

(45) Chen, F.; Lam, C.-H.; Tsui, O. K. C. The Surface Mobility of Glasses. *Science* **2014**, *343* (6174), 975–976. https://doi.org/10.1126/science.1248113.

(46) Glor, E. C.; Fakhraai, Z. Facilitation of Interfacial Dynamics in Entangled Polymer Films. *J. Chem. Phys.* **2014**, *141* (19), 194505. https://doi.org/10.1063/1.4901512.

(47) Yang, Z.; Fujii, Y.; Lee, F. K.; Lam, C.-H.; Tsui, O. K. C. Glass Transition Dynamics and Surface Layer Mobility in Unentangled Polystyrene Films. *Science* **2010**, *328* (5986), 1676–1679. https://doi.org/10.1126/science.1184394.

(48) Xia, W.; Hsu, D. D.; Keten, S. Molecular Weight Effects on the Glass Transition and Confinement Behavior of Polymer Thin Films. *Macromol. Rapid Commun.* **2015**, *36* (15), 1422–1427. https://doi.org/10.1002/marc.201500194.

(49) Diaz-Vela, D.; Hung, J.-H.; Simmons, D. S. Temperature-Independent Rescaling of the Local Activation Barrier Drives Free Surface Nanoconfinement Effects on Segmental-Scale Translational Dynamics near Tg. *ACS Macro Lett.* **2018**, 1295–1301. https://doi.org/10.1021/acsmacrolett.8b00695.

(50) Kremer, K.; Grest, G. S. Molecular Dynamics (MD) Simulations for Polymers. *J. Phys. Condens. Matter* **1990**, *2* (S), SA295–SA298.

(51) Mackura, M. E.; Simmons, D. S. Enhancing Heterogenous Crystallization Resistance in a Bead-Spring Polymer Model by Modifying Bond Length. *J. Polym. Sci. Part B Polym. Phys.* **2014**, *52* (2), 134–140. https://doi.org/10.1002/polb.23398.

(52) Ruan, D.; Simmons, D. S. Roles of Chain Stiffness and Segmental Rattling in Ionomer Glass Formation. *J. Polym. Sci. Part B Polym. Phys.* **2015**, *53* (20), 1458–1469. https://doi.org/10.1002/polb.23788.

(53) Mangalara, J. H.; Simmons, D. S. Tuning Polymer Glass Formation Behavior and Mechanical Properties with Oligomeric Diluents of Varying Stiffness. *ACS Macro Lett.* **2015**, *4* (10), 1134–1138. https://doi.org/10.1021/acsmacrolett.5b00635.

(54) Shavit, A.; Riggleman, R. A. Physical Aging, the Local Dynamics of Glass-Forming Polymers under Nanoscale Confinement. *J. Phys. Chem. B* **2014**, *118* (30), 9096–9103. https://doi.org/10.1021/jp502952n.

(55) Baschnagel, J.; Varnik, F. Computer Simulations of Supercooled Polymer Melts in the Bulk and in Confined Geometry. *J. Phys. Condens. Matter* **2005**, *17* (32), R851–R953. https://doi.org/10.1088/0953-8984/17/32/R02.

(56) Kremer, K.; Grest, G. S. Dynamics of Entangled Linear Polymer Melts: A Molecular-dynamics Simulation. *J. Chem. Phys.* **1990**, *92* (8), 5057–5086. https://doi.org/doi:10.1063/1.458541.

(57) Slimani, M. Z.; Moreno, A. J.; Colmenero, J. Heterogeneity of the Segmental Dynamics in Lamellar Phases of Diblock Copolymers. *Macromolecules* **2011**, *44* (17), 6952–6961. https://doi.org/10.1021/ma200470a.

(58) Plimpton, S. J. Fast Parallel Algorithms for Short-Range Molecular Dynamics. *J Comp Phys* **1995**, *117*, 1–19.

(59) Hung, J.-H.; Patra, T. K.; Meenakshisundaram, V.; Mangalara, J. H.; Simmons, D. S. Universal Localization Transition Accompanying Glass Formation: Insights from Efficient Molecular Dynamics Simulations of Diverse Supercooled Liquids. *Soft Matter* **2018**, *15*, 1223–1242. https://doi.org/10.1039/C8SM02051E.

(60) Cheng, Y.; Yang, J.; Hung, J.-H.; Patra, T. K.; Simmons, D. S. Design Rules for Highly Conductive Polymeric Ionic Liquids from Molecular Dynamics Simulations. *Macromolecules* **2018**, *51* (17), 6630–6644. https://doi.org/10.1021/acs.macromol.8b00572.

(61) Hung, J.-H.; Mangalara, J. H.; Simmons, D. S. Heterogeneous Rouse Model Predicts Polymer Chain Translational Normal Mode Decoupling. *Macromolecules* **2018**, *51* (8), 2887–2898. https://doi.org/10.1021/acs.macromol.8b00135.

(62) Meenakshisundaram, V.; Hung, J.-H.; Simmons, D. S. Design Rules for Glass Formation from Model Molecules Designed by a Neural-Network-Biased Genetic Algorithm. *Soft Matter* **2019**, *15*, 7795–7808. https://doi.org/10.1039/C9SM01486A.

(63) Williams, G.; Watts, D. C. Non-Symmetrical Dielectric Relaxation Behaviour Arising from a Simple Empirical Decay Function. *Trans Faraday Soc* **1970**, *66*, 80–85. https://doi.org/10.1039/TF9706600080.

(64) Kohlrausch, F. Kohlrausch. *Pogg Ann Phys.* **1863**, *119*, 352.

(65) Hanakata, P. Z.; Douglas, J. F.; Starr, F. W. Local Variation of Fragility and Glass Transition Temperature of Ultra-Thin Supported Polymer Films. *J. Chem. Phys.* **2012**, *137* (24), 244901. https://doi.org/doi:10.1063/1.4772402.

(66) Ruan, D.; Simmons, D. S. Glass Formation near Covalently Grafted Interfaces: Ionomers as a Model Case. *Macromolecules* **2015**, *48* (7), 2313–2323. https://doi.org/10.1021/acs.macromol.5b00025.

(67) Lee, J.; Mangalara, J. H.; Simmons, D. S. Correspondence between the Rigid Amorphous Fraction and Nanoconfinement Effects on Glass Formation. *J. Polym. Sci. Part B Polym. Phys.* **2017**, *55* (12), 907–918. https://doi.org/10.1002/polb.24324.

(68) Forrest, J. A.; Dalnoki-Veress, K. The Glass Transition in Thin Polymer Films. *Adv. Colloid Interface Sci.* **2001**, *94* (1–3), 167–195. https://doi.org/10.1016/S0001-8686(01)00060-4.

(69) Simmons, D. S.; Cicerone, M. T.; Zhong, Q.; Tyagi, M.; Douglas, J. F. Generalized Localization Model of Relaxation in Glass-Forming Liquids. *Soft Matter* **2012**, *8* (45), 11455–11461. https://doi.org/10.1039/c2sm26694f.

(70) Kivelson, D.; Tarjus, G.; Zhao, X.; Kivelson, S. A. Fitting of Viscosity: Distinguishing the Temperature Dependences Predicted by Various Models of Supercooled Liquids. *Phys. Rev. E* **1996**, *53* (1), 751–758. https://doi.org/10.1103/PhysRevE.53.751.

(71) Schmidtke, B.; Hofmann, M.; Lichtinger, A.; Rössler, E. A. Temperature Dependence of the Segmental Relaxation Time of Polymers Revisited. *Macromolecules* **2015**, *48* (9), 3005–3013. https://doi.org/10.1021/acs.macromol.5b00204.

(72) Mirigian, S.; Schweizer, K. S. Elastically Cooperative Activated Barrier Hopping Theory of Relaxation in Viscous Fluids. I. General Formulation and Application to Hard Sphere Fluids. *J. Chem. Phys.* **2014**, *140* (19), 194506. https://doi.org/10.1063/1.4874842.

(73) Dyre, J. C. Colloquium: The Glass Transition and Elastic Models of Glass-Forming Liquids. *Rev. Mod. Phys.* **2006**, *78* (3), 953–972. https://doi.org/Review.

(74) Adam, G.; Gibbs, J. H. On the Temperature Dependence of Cooperative Relaxation Properties in Glass-Forming Liquids. *J Chem Phys* **1965**, *43* (1), 139–146.

(75) Sussman, D. M.; Schoenholz, S. S.; Cubuk, E. D.; Liu, A. J. Disconnecting Structure and Dynamics in Glassy Thin Films. *Proc. Natl. Acad. Sci.* **2017**, *114* (40), 10601–10605. https://doi.org/10.1073/pnas.1703927114.

(76) Mirigian, S.; Schweizer, K. S. Elastically Cooperative Activated Barrier Hopping Theory of Relaxation in Viscous Fluids. II. Thermal Liquids. *J. Chem. Phys.* **2014**, *140* (19), 194507. https://doi.org/10.1063/1.4874843.

(77) Schmidtke, B.; Petzold, N.; Kahlau, R.; Hofmann, M.; Rössler, E. A. From Boiling Point to Glass Transition Temperature: Transport Coefficients in Molecular Liquids Follow Three-Parameter Scaling. *Phys. Rev. E* **2012**, *86* (4), 041507. https://doi.org/10.1103/PhysRevE.86.041507.

(78) Petzold, N.; Schmidtke, B.; Kahlau, R.; Bock, D.; Meier, R.; Micko, B.; Kruk, D.; Rössler, E. A. Evolution of the Dynamic Susceptibility in Molecular Glass Formers: Results from Light Scattering, Dielectric Spectroscopy, and NMR. *J. Chem. Phys.* **2013**, *138* (12), 12A510. https://doi.org/10.1063/1.4770055.

(79) Zhou, Y.; Milner, S. T. Short-Time Dynamics Reveals Tg Suppression in Simulated Polystyrene Thin Films. *Macromolecules* **2017**, *50* (14), 5599–5610. https://doi.org/10.1021/acs.macromol.7b00921.

(80) Xia, W.; Keten, S. Coupled Effects of Substrate Adhesion and Intermolecular Forces on Polymer Thin Film Glass-Transition Behavior. *Langmuir* **2013**, *29* (41), 12730–12736. https://doi.org/10.1021/la402800j.

(81) Hsu, D. D.; Xia, W.; Song, J.; Keten, S. Glass-Transition and Side-Chain Dynamics in Thin Films: Explaining Dissimilar Free Surface Effects for Polystyrene vs Poly(Methyl Methacrylate). *ACS Macro Lett.* **2016**, *5* (4), 481–486. https://doi.org/10.1021/acsmacrolett.6b00037.

(82) Glor, E. C.; Angrand, G. V.; Fakhraai, Z. Exploring the Broadening and the Existence of Two Glass Transitions Due to Competing Interfacial Effects in Thin, Supported Polymer Films. *J. Chem. Phys.* **2017**, *146* (20), 203330. https://doi.org/10.1063/1.4979944.

(83) Zhang, Y.; Woods, C. N.; Alvarez, M.; Jin, Y.; Riggleman, R. A.; Fakhraai, Z. Effect of Substrate Interactions on the Glass Transition and Length-Scale of Correlated Dynamics in Ultra-Thin Molecular Glass Films. *J. Chem. Phys.* **2018**, *149* (18), 184902. https://doi.org/10.1063/1.5038174.

(84) Chowdhury, M.; Guo, Y.; Wang, Y.; Merling, W. L.; Mangalara, J. H.; Simmons, D. S.; Priestley, R. D. Spatially Distributed Rheological Properties in Confined Polymers by Noncontact Shear. *J. Phys. Chem. Lett.* **2017**, 1229–1234. https://doi.org/10.1021/acs.jpclett.7b00214.

(85) Pye, J. E.; Roth, C. B. Two Simultaneous Mechanisms Causing Glass Transition Temperature Reductions in High Molecular Weight Freestanding Polymer Films as Measured by Transmission Ellipsometry. *Phys. Rev. Lett.* **2011**, *107* (23), 235701. https://doi.org/10.1103/PhysRevLett.107.235701.

(86) Napolitano, S.; Wübbenhorst, M. Structural Relaxation and Dynamic Fragility of Freely Standing Polymer Films. *Polymer* **2010**, *51* (23), 5309–5312. https://doi.org/10.1016/j.polymer.2010.09.060.

(87) Phan, A. D.; Schweizer, K. S. Dynamic Gradients, Mobile Layers, Tg Shifts, Role of Vitrification Criterion, and Inhomogeneous Decoupling in Free-Standing Polymer Films. *Macromolecules* **2018**, *51* (15), 6063–6075. https://doi.org/10.1021/acs.macromol.8b01094.